P-Band Radar Retrieval of Subsurface Soil Moisture Profile as a Second-Order Polynomial: First AirMOSS Results

Alireza Tabatabaeenejad, *Senior Member, IEEE*, Mariko Burgin, *Member, IEEE*, Xueyang Duan, *Member, IEEE*, and Mahta Moghaddam, *Fellow, IEEE*

***Abstract*—We propose a new model for estimating subsurface soil moisture using P-band radar data over barren, shrubland, and vegetated terrains. The unknown soil moisture profile is assumed to have a second-order polynomial form as a function of subsurface depth with three unknown coefficients that we estimate using the simulated annealing algorithm. These retrieved coefficients produce the value of soil moisture at any given depth up to a prescribed depth of validity. We use a discrete scattering model to calculate the radar backscattering coefficients of the terrain. The retrieval method is tested and developed with synthetic radar data and is validated with measured radar data and *in situ* soil moisture measurements. Both forward and inverse models are briefly explained. The radar data used in this paper have been collected during the Airborne Microwave Observatory of Subcanopy and Subsurface (AirMOSS) mission flights in September and October of 2012 over a 100 km by 25 km area in Arizona, including the Walnut Gulch Experimental Watershed. The study area and the ancillary data layers used to characterize each radar pixel are explained. The inversion results are presented, and it is shown that the RMSE between the retrieved and measured soil moisture profiles ranges from 0.060 to 0.099 $\mathrm{m}^3/\mathrm{m}^3$, with a Root Mean Squared Error (RMSE) of 0.075 $\mathrm{m}^3/\mathrm{m}^3$ over all sites and all acquisition dates. We show that the accuracy of retrievals decreases as depth increases. The profiles used in validation are from a fairy dry season in Walnut Gulch and so are the accuracy conclusions.**

***Index Terms*—Airborne Microwave Observatory of Subcanopy and Subsurface (AirMOSS), discrete scattering model, quadratic function, radar, remote sensing, second-order polynomial, simulated annealing, soil moisture profile.**

I. Introduction

SOIL moisture is a key variable of the Earth system due to its role in connecting the processes between the land surface and the atmosphere. Soil moisture links the water and carbon cycles through the vegetation cover and its roots. It has been shown that there is strong feedback between the soil moisture anomalies and climate [1]. Mapping of the global soil moisture can therefore improve our understanding of the global water, energy, and carbon cycles, as well as the climate. The importance of global soil moisture maps has motivated missions such as the NASA Soil Moisture Active and Passive (SMAP) mission [2], NASA Earth Ventures 1 (EV-1) Airborne Microwave Observatory of Subcanopy and Subsurface (AirMOSS) [3], and the European Space Agency (ESA) Soil Moisture and Ocean Salinity (SMOS) [4].

Since the 1970s, the effects of soil moisture on the scattered electromagnetic waves have been studied [5]. All along, microwave-based retrieval of soil moisture has remained a challenging problem due to modeling complexity of the vegetation canopy, land topography, and soil layers. Several empirical and theoretical forward models have been developed for both bare and vegetated surfaces, including models that use empirical functions based on measured data [6], [7] or models that use fitted functions based on synthesized radar data [8], [9]. If the forward model has a simple invertible functional form, the inversion is straightforward [9], but for more complicated models without direct inverses, methods such as nonlinear optimization [10] or data cube searches [11] have been used for inversion. Bayesian estimation methods are other inversion techniques that use conditional density functions to find an optimum estimator that minimizes the RMSE [12]. Some inversion techniques, including time series [13], [14] and change detection [15], are based on temporal variation of soil moisture under the assumption that surface roughness and vegetation water content do not change appreciably during successive observations. Both methods assume a linear relation between soil moisture and logarithm of the radar backscattering coefficient (i.e., the backscattering coefficient in the dB scale).

The aforementioned techniques, excluding that in [10], model the soil as a homogeneous half-space and retrieve only one effective value for the soil moisture. However, considering a layered dielectric structure, if a single soil moisture value is retrieved, it will not necessarily be representative of any layer's soil moisture. Additionally, as shown in this paper, one retrieved soil moisture value does not correspond to any unique or meaningful linear averaging scheme over the moisture contents of the layers. While there might exist a nonlinear averaging scheme, particularly for cases with different layer thicknesses, such a scheme would be a function of the profile shape, and a unique averaging scheme that is applicable to a large range of profiles cannot be defined. Moreover, and most importantly, we are interested in the soil moisture content of individual layers at several depths up to the root zone. Clearly, one average value cannot uniquely represent multiple soil moisture contents.

Manuscript received May 24, 2013; revised December 5, 2013 and March 22, 2014; accepted May 2, 2014. Date of publication June 18, 2014; date of current version August 12, 2014.

A. Tabatabaeenejad and M. Moghaddam are with the Ming Hsieh Department of Electrical Engineering, University of Southern California, Los Angeles, CA 90089 USA.

M. Burgin and X. Duan are with the Jet Propulsion Laboratory, California Institute of Technology, Pasadena, CA 91109 USA.

Color versions of one or more of the figures in this paper are available online at http://ieeexplore.ieee.org.

Digital Object Identifier 10.1109/TGRS.2014.2326839

There have been several studies on the retrieval of a soil moisture profile from both active and passive remote sensing observations. These studies have either been limited to retrieval of soil moisture of the first few centimeters of soil [16] or to retrieval of the soil moisture profile from surface soil moisture using sequential data-assimilation techniques [17]–[19]. When direct retrieval of root-zone soil moisture (RZSM) has been studied, the models have used data cubes for specific soil conditions [20], [21]. Nonetheless, direct retrieval of RZSM under vegetation canopies using active remote sensing data (either real or synthesized) has not been studied, although it has been shown that deeper soil moisture can impact the radar response significantly [22]–[24]. In this paper, we propose a method to use real radar signal at P-band to retrieve the soil moisture profile without limiting the technique to any specific site or soil.

The number of synthetic aperture radar (SAR) observations (in terms of frequency, polarization channels, and incidence angles) is usually limited. For example, for AirMOSS measurements, there are up to three independent polarization channels (i.e., HH, VV, HV), one frequency band (namely 420–440 MHz, with the center frequency of 430 MHz), and one incidence angle in the range of 25°–55°.[1] Therefore, regardless of the scattering and inversion models used, the estimation of RZSM, whether in barren or vegetated surfaces, is challenging, and we would have to minimize the number of unknown parameters commensurately with the number of measured data points. Moreover, by definition, RZSM needs to be known at depths that would only be reached if several layers are included in the retrieval process. Therefore, we need a method of estimating the moisture contents of layers that can be used to retrieve meaningful values representing surface and subsurface moisture without introducing a large number of unknowns. Since it is not feasible to define the unknowns as the soil moisture contents of the individual soil layers, one solution would be to parameterize the moisture profile and estimate these parameters. Several functions can be identified as representatives of soil moisture, namely linear, piecewise linear, exponential, and parabolic [25]. Moreover, physics-based profiles can also be found by solving, via our optimization method, the differential equation that governs the steady-state vertical flux [26].

In this paper, we propose a second-order polynomial function. Accordingly, the moisture profile has the form of $az^2 + bz + c$, where z is the depth below surface, and a, b, and c are the coefficients to be retrieved from radar measurements. A preliminary version of this concept has been reported previously [27], but it was not sufficiently developed or validated with AirMOSS data. The choice of quadratic function is just a beginning step toward retrieving functions that are representative of the entire profile while other aforementioned possibilities warrant extensive study, which is part of our future work.

The parameters that characterize a radar pixel are the vegetation parameters and soil texture information, which are described later. In this paper, we assume the soil profile is the only unknown and consider every other parameter (namely vegetation parameters, and soil texture and structural information) as known. In particular, we assume *a priori* soil roughness information is available from field measurements. Soil roughness has been a parameter of interest in many remote sensing studies due to its influence on the radar signal [6], [9]. However, in this paper and in current AirMOSS data processing, due to the limited number of SAR observations compared with the number of unknowns, we consider roughness a known parameter and fixed for each land cover type within a site. We will mention later that the entire parameterization is validated by comparing the output of the forward model against radar data over several pixels within the same scene.

The choice of the P-band frequency allows the electromagnetic wave to penetrate the canopy and soil easily. The soil penetration depth (defined as the distance over which the wave amplitude decays to $1/e$ or -8.7 dB of its original value) is greater than 2 m at 435 MHz for a typical sandy soil with a volumetric moisture content of 0.25 $\mathrm{m}^3/\mathrm{m}^3$ [28], giving us confidence to reach the root zone in the retrieval process.[2]

This paper is organized as follows. Section II presents a brief overview of the AirMOSS project and its radar instrument and data. In Section III, we examine the accuracy of a second-order polynomial fit for several cases of soil moisture profiles in AirMOSS sites. In Section IV, we elaborate the insufficiency of single-value retrieval in soil moisture estimation problems, and particularly for the P-band AirMOSS. The retrieval algorithm and the forward model are described in Section V, followed by a brief description of ancillary data handling and processing in Section VI. (More details on the data handling processor will be provided in a separate paper.) The inversion results are presented in Section VII for both synthetic and measured radar data. Conclusion and summary remarks follow in Section VIII.

II. AirMOSS Project and Radar Instrument

The AirMOSS mission seeks to improve the estimates of the North American Net Ecosystem Exchange (NEE) by: 1) providing high-resolution observations of RZSM over nine regions representative of the major North American biomes; 2) estimating the impact of RZSM on regional carbon fluxes; and 3) integrating the measurement-constrained estimates of regional carbon fluxes to the continental scale of North America [3]. AirMOSS flies a P-band SAR in order to penetrate vegetation and into the root zone to provide estimates of RZSM. The flights cover areas of approximately 100 km by 25 km containing FLUXNET tower sites in regions ranging from boreal forests in Saskatchewan, Canada, to tropical forests in La Selva, Costa Rica. The radar snapshots are used to generate estimates of RZSM via inversion of scattering models of vegetation overlying soils with variable moisture profiles. These retrievals will in turn be assimilated or otherwise used by hydrologists to estimate land model hydrological parameters over the nine

[1]For some narrow areas that are overlaps of two flight lines, there might be two look angles available for the inversion algorithm, but these areas are very small portions of the entire flown area.

[2]The approach we have used in this paper is not applicable to SMAP observations as SMAP is an L-band mission incapable of sensing deep soil moisture. Our work is, however, beneficial in the validation and accuracy assessment of the SMAP Level 4 products.

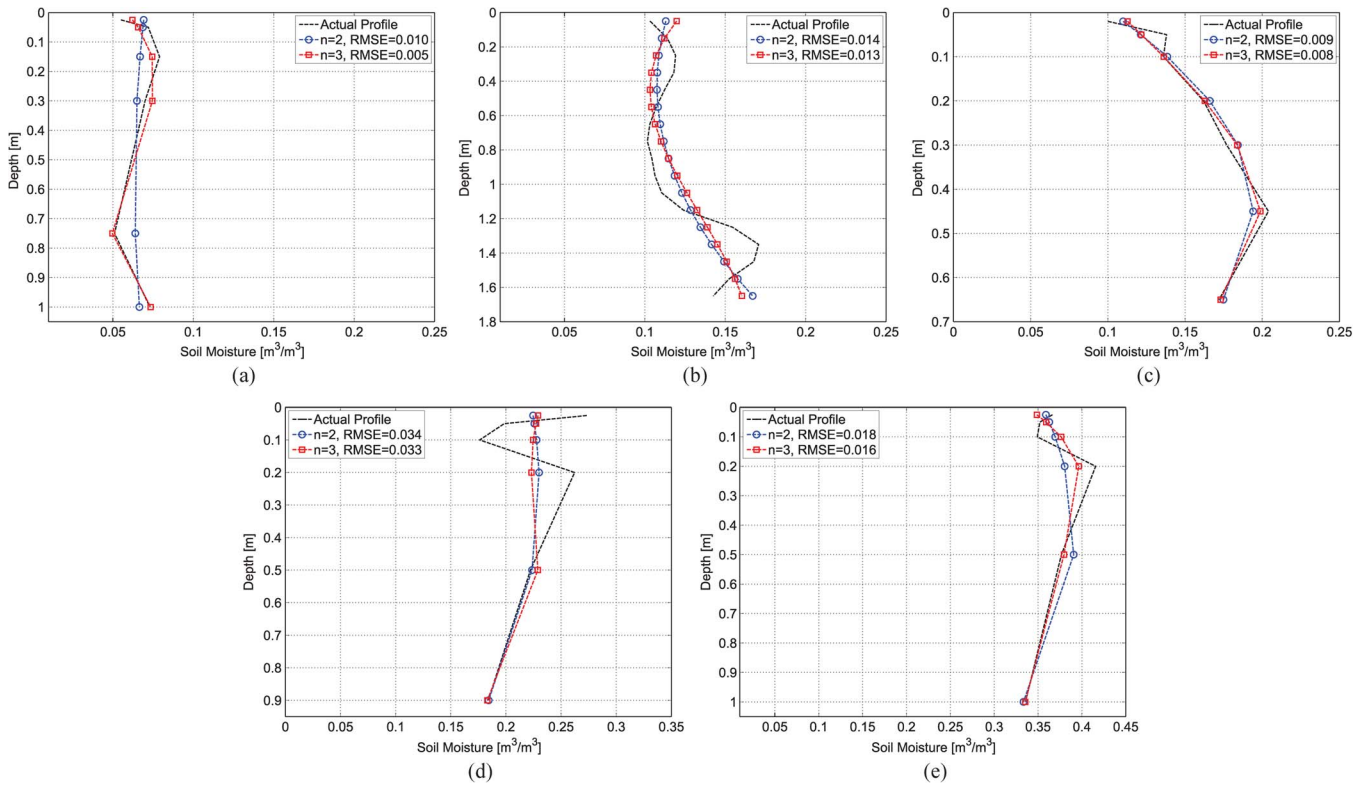

Fig. 1. Measured moisture profiles and their second- and third-order polynomial fits at locations close to the flux towers in (a) Walnut Gulch from September 20, 2012, (b) BOREAS OJP from July 29, 1994, (c) Tonzi Ranch from January 8, 2012, (d) MOISST from October 14, 2012, and (d) MOISST from April 15, 2012. The RMSEs show that a second-order fit meets the AirMOSS error criterion of an absolute RMSE of less than 0.05 $\mathrm{m}^3/\mathrm{m}^3$.

biomes, generating a fine-grained time record of soil moisture evolution in the root zone. These hydrological parameters will ultimately be integrated with an ecosystem demography model to predict the respiration and photosynthesis carbon fluxes.

The AirMOSS radar is based on JPL's L-band Uninhabited Aerial Vehicle SAR (UAVSAR) system. The AirMOSS P-band SAR uses UAVSAR's existing L-band RF and digital electronics subsystems, but new upconverters and down-converters convert the L-band signals to ultrahigh frequencies (i.e., 280–440 MHz). The project requirements for relative and absolute calibration accuracy levels are 1 (i.e., ± 0.5) and 1.5 (i.e., ± 0.75) dB, respectively.[3] These accuracy values have been achieved based on the analysis of 4.8-m trihedral corner reflector data. The variability seen in the radar data from our calibration site (in Rosamond dry lake bed in California) implies that we have data-take-to-data-take radiometric biases. Based on the calibration site data, collected on multiple days spread over a period of over a year, the bias from one day to another is the similar size as the bias from one data take to another on the same day. The calibration stability associated with these data is estimated at 0.6 dB. Moreover, the speckle noise (i.e., signal standard deviation normalized to its mean value) at the 0.5- and 3-arcsecond spatial resolution at the Walnut Gulch site (our study site in this paper) is, respectively, $\simeq -11.3$ and $\simeq -18.9$ dB, given $\sigma^o \simeq -40$ dB, where σ^o is the system's noise-equivalent sigma nought.

The project and its radar system are respectively detailed in the project Web site [3] and in a previous AirMOSS publication by Chapin *et al.* [29].

III. Polynomial Fit of Soil-Moisture Profile

To examine whether it is reasonable to assume moisture profiles can be approximated with a second-order polynomial, we have studied the moisture data, ranging from very dry to very wet, from four AirMOSS sites. Fig. 1 shows five examples of soil moisture profile from these sites. Fig. 1(a) shows a profile from September 20, 2012 in Lucky Hills Shrubland in the Walnut Gulch Experimental Watershed, AZ. Fig. 1(b) shows a similar profile from May 25, 1994, in an old Jack pine (OJP) forest of the Boreal Ecosystem–Atmosphere Study (BOREAS) site in Saskatchewan, Canada, which is also one of the AirMOSS sites [30]. Fig. 1(c) shows a moisture profile from January 8, 2012 in a location close to the flux tower at the Tonzi Ranch site of AirMOSS, located near Sacramento, CA, with a woody Savanna land cover type. Finally, Fig. 1(d) and (e) show two examples from October 14 and April 15, 2012, respectively, in the MOISST site in Oklahoma with mostly grassland or bare soil. The RMSE is small for the polynomial fits of the shown orders and meets the AirMOSS error criterion of an absolute RMSE of less than 0.05 $\mathrm{m}^3/\mathrm{m}^3$. This RMSE should ultimately be calculated over all AirMOSS sites and all dates.

[3]The relative calibration accuracy refers to an intrascene variation of the radar data, whereas the absolute calibration accuracy refers to deviation of the radar data from the true values. Both accuracy values are measured within the same date take over the calibration site.

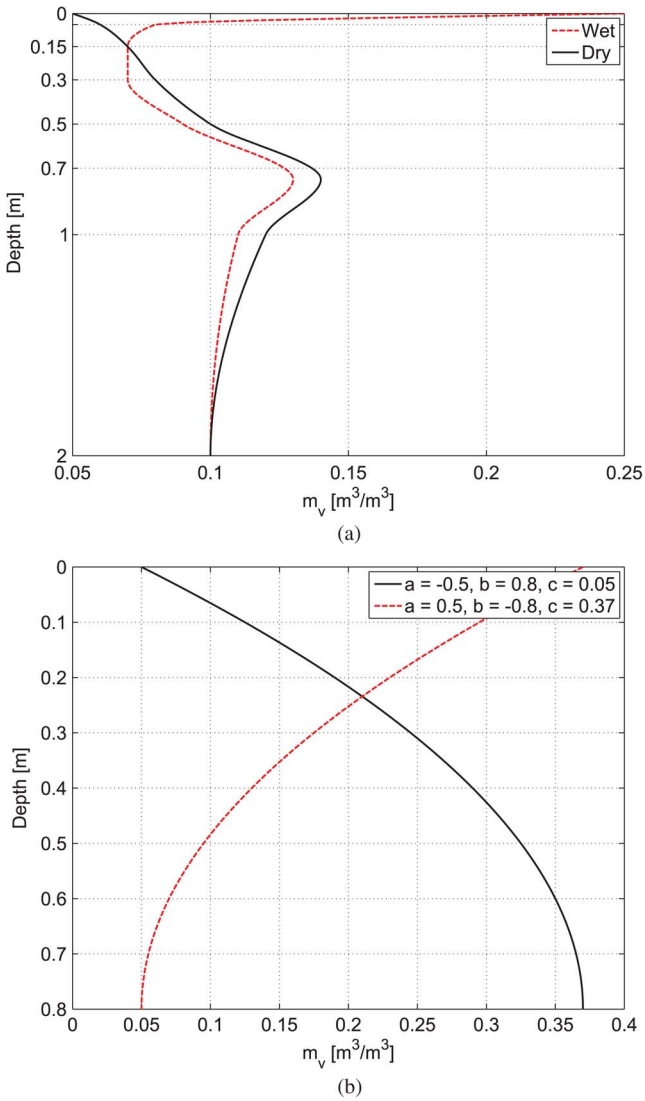

Fig. 2. (a) Two measured moisture profiles in Arizona's Lucky Hills from 2003. The actual measurement points are 5, 15, 30, 50, 70, 100, and 200 cm. (b) Two nominal examples of quadratic profiles: increasing moisture with depth and decreasing moisture with depth.

We should mention that, depending on the site and its infiltration dynamics, a higher-order polynomial may be a more accurate representative of the moisture profile. Upon the availability of more SAR observations (in terms of frequency or incidence angle), and depending on the site, it is possible to use a higher order polynomial in the future.

IV. Linear Averaging of Soil-Moisture Profile

We mentioned in Section I that in an inverse problem associated with a layered dielectric structure, *one* retrieved soil moisture value is an inaccurate representation of the linear average over the dielectric constants (or moisture contents) of the layers. We now provide an elaboration of this statement using synthetic radar data.

Consider the profiles shown in Fig. 2(a). These real profiles are from a field campaign by the University of Arizona and the U.S. Department of Agriculture Agricultural Research Service (USDA-ARS) Southwest Watershed Research Center in September 2003 to measure soil moisture in Arizona's Lucky Hills in support of the Microwave Observatory of Subcanopy and Subsurface (MOSS) project [31].[4] We investigate the retrieval accuracy when *one* value is retrieved as the "effective" soil moisture content. To synthesize radar data, we use the small perturbation method (SPM) model of [22] assuming bare soil. The soil is modeled with an eight-layer geometry with the layer boundaries located at 5, 15, 30, 50, 70, 100, and 200 cm. These depths are the actual and only measurement points in the profile; therefore, for simulation of the radar data, we would have to assume an eight-layer geometry.[5] We also assume there are no distinct soil horizons, hence uniform soil texture across all layers. For our statistical study, 300 realizations of the geometry are generated, and for each realization, the soil moisture contents of all layers are perturbed to generate a new profile, hence a new set of radar data. The simulated annealing method, explained in Section V, is then applied to retrieve one "effective" soil moisture value from each realization. The same forward model is used in data synthesis and cost function evaluation in the optimization scheme. Fig. 3 shows a comparison between the output of the inversion algorithm and linear averages of the moisture contents of up to four layers of the corresponding eight-layer geometry. We observe that the RMSE is "small" for the dry profile, but for the case of the wet profile, the RMSE is "large," confirming that a single retrieved value for soil moisture is not representative of any layer soil moisture nor does it correspond to any linear averaging scheme over the layers moisture contents.[6]

However, depending on the profile, a linear average value may accurately represent the single retrieved value. For example, Fig. 2(b) shows two examples of quadratic profiles with the coefficients $a = -0.5$, $b = 0.8$, and $c = 0.05$, for a profile with increasing moisture with depth, and $a = 0.5$, $b = -0.8$, and $c = 0.37$, for a profile with decreasing moisture with depth. Similar to the previous analysis, to synthesize the radar data, we discretize the profiles. For this analysis, to capture all variations in the profile, we discretize it with 20 layers with a thickness of 5 cm for each. For each of the 300 realizations, the coefficients a, b, and c are perturbed independently to generate a new profile and a new set of radar data. The simulated annealing method is then applied to retrieve one soil moisture value, and then a comparison is made between the retrieved soil moisture value and several linear averages. Fig. 4 shows the result. It is evident that while all of the presented average values generate a small RMSE, there is an optimum number of layers that would generate the best estimation of the retrieved soil moisture.

Based on the simulations presented in this section, we can conclude that there is no unique linear averaging scheme that can represent a single retrieved value for soil moisture. We cannot claim that no other averaging scheme (such as nonlinear or weighted linear) does so, but even if such a scheme exists, the soil moisture profile cannot be constructed from it. Since

[4]The moisture information is available for the period of September 13–29, 2003. Based on these data, the soil condition was fairly dry until September 23, 2003, when a rainfall happened. The "Wet" profile was measured after that day.

[5]Although deep layers would have negligible contribution to the synthetic radar data, they are included in the simulation for accuracy.

[6]Our measure for largeness and smallness of RMSE is the AirMOSS project criterion of 0.05 m^3/m^3.

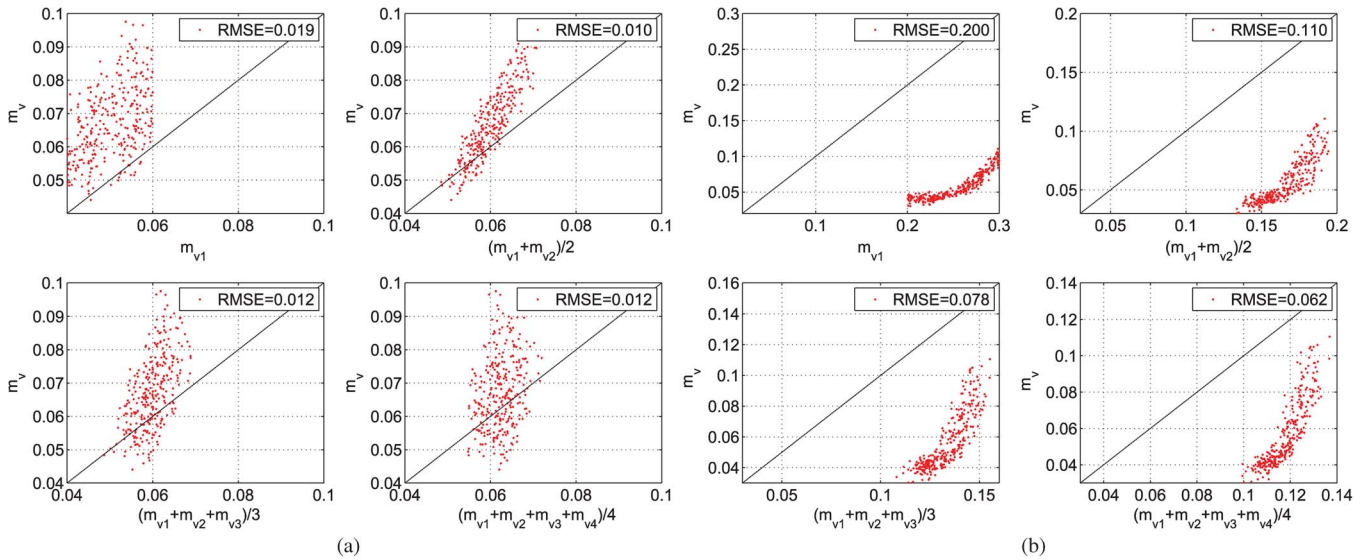

Fig. 3. Single output of the inversion algorithm versus linear averages of the moisture contents of up to four layers for the profiles shown in Fig. 2(a). See Section IV for details. The RMSE is large for the wet profile, confirming that a single retrieved value for soil moisture is not representative of any layer soil moisture nor does it correspond to any linear averaging scheme over the layers moisture contents. (a) Dry profile. (b) Wet profile.

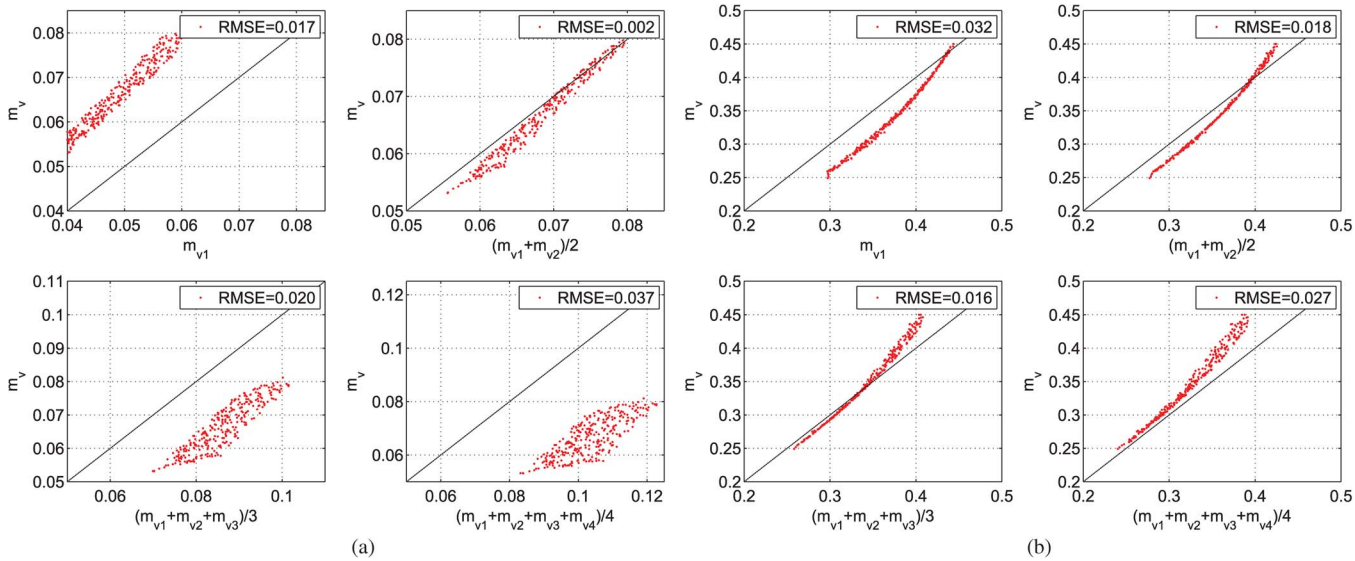

Fig. 4. Single output of the inversion algorithm versus linear averages of the moisture contents of up to four layers for the profiles shown in Fig. 2(b). See Section IV for details. The RMSE is small for both profiles and there is an optimum number of averaged layers that would generate the best estimation of the retrieved soil moisture. (a) Dry profile. (b) Wet profile.

the thrust of this paper is the retrieval of the moisture profile up to a prescribed depth (that will be elaborated later), we will estimate the moisture contents of several layers by retrieving the unknown coefficients of the second-order polynomial that represents the moisture profile.

V. Forward and Retrieval Models

Since all of the AirMOSS sites include vegetated areas, we use a discrete radar scattering model to model the scattering of electromagnetic waves at these sites. The model assumes single-species vegetation with horizontal homogeneity within a radar pixel while allowing vertical heterogeneity by introducing a stem layer and a canopy layer [32], [33]. The stem layer is represented by nearly vertical dielectric cylinders. The canopy layer contains randomly distributed large and small dielectric cylinders representing large and small branches. The canopy layer also contains leaves, which are randomly but uniformly distributed in the layer. Leaves are represented by disks or cylinders depending on the type of the forest, i.e., deciduous or coniferous. The forest floor is modeled as a layered dielectric structure characterized by the interface roughness and layer dielectric constants and thickness. The roots are not taken into account in this model. The radar model identifies several scattering mechanisms: scattering from crown layer, scattering from trunks, double-bounce scattering between the crown layer and ground, double-bounce scattering between the trunks and ground, and backscattering from the ground. These mechanisms are illustrated in Fig. 5(a). The total backscattered power, represented by the Stokes (or Mueller) matrix, is the

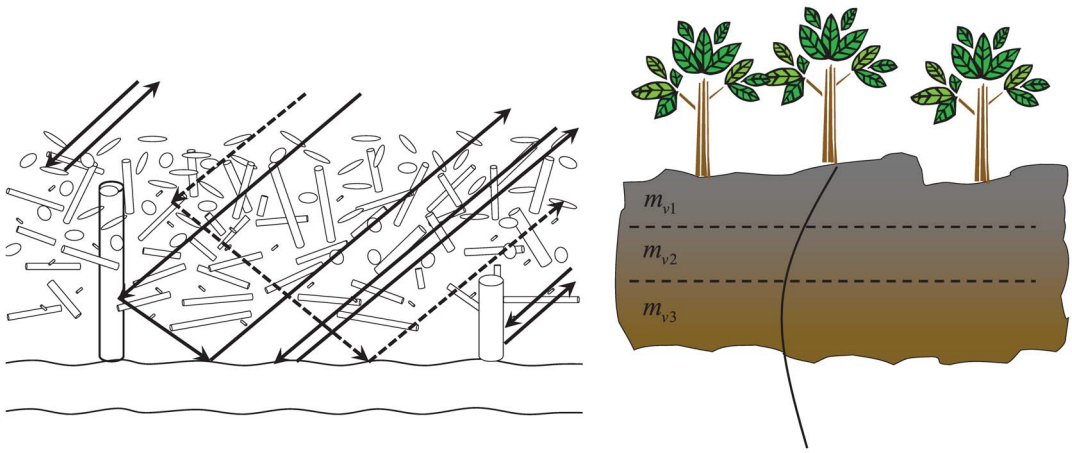

Fig. 5. (a) Scattering mechanisms present in the forward model. (b) Forest geometry and moisture profile that is assumed a quadratic function, i.e., $az^2 + bz + c$, where z is the depth, and a, b, and c are the coefficients to be retrieved from radar measurements.

sum of the power from all contributing scatterers [32]. The total Stokes matrix is

$$\mathbf{M_{tot}} = \mathbf{M_b} + \mathbf{T_b}\mathbf{M_t}\mathbf{T_b} + \mathbf{T_b}\mathbf{T_t}\mathbf{M_{bg}}\mathbf{T_t}\mathbf{T_b} + \mathbf{T_b}\mathbf{T_t}\mathbf{M_{tg}}\mathbf{T_t}\mathbf{T_b} + \mathbf{T_b}\mathbf{T_t}\mathbf{M_g}\mathbf{T_t}\mathbf{T_b} \quad (1)$$

where $\mathbf{T}$ denotes transition Stokes matrix and $\mathbf{M}$ denotes backscatter Stokes matrix. The subscripts "$\mathbf{b}$ ", "$\mathbf{t}$", and "$\mathbf{g}$" denote "branch," "trunk," and "ground," respectively.

It has been shown that, at low frequencies, the trunk-ground double-bounce process is the mechanism primarily responsible for the backscattering signal over forests with tall stands [8]. We also mentioned earlier that, in a layered rough surface structure, a subsurface layer contribution to the backscattering from ground and to the ground-trunk double-bounce scattering process can be significant. Therefore, to include the coherent multiple scattering effects within soil layers in the modeling of double bounces, we have integrated a layered-soil scattering model into the forest scattering model of [34]. We have used the layered SPM of [22] for the backscattering from ground, whereas the N-layer version of the coherent scattering model of [24] has been used for the trunk-ground double-bounce mechanism. This extended model will be published in future work.

The forward model uses several parameters to characterize a vegetated area. These parameters are the properties of large and small branches (dielectric constant, length, radius, density, and orientation), leaves (dielectric constant, length, radius, and density), trunks (dielectric constant, length, radius, and density), soil (volumetric moisture content, roughness RMS height) and canopy height. The orientation of small and large branches is described by species-specific probability density functions (PDFs). The AirMOSS sites are divided into single-species and multi-species sites. The focus of this paper is on the single-species vegetation sites, but for the future, the full complexity of realistic vegetation can be included if necessary [33]. The parameters necessary to define the scene are based on readily available ancillary data, described in Section VI, as well as ground measurements. Fig. 5(b) shows the forest geometry and the moisture profile that is assumed to have a second-order polynomial form.

To estimate the unknown coefficients of the second-order polynomial, namely a, b, and c, we use simulated annealing [10], [35] to minimize a cost function that is based on the difference between measured and calculated backscattering coefficients, and is defined as

$$L(\mathbf{X}) = \sum_{pq} \left(\frac{10 \log \sigma^o_{pq}(\mathbf{X}; \mathbf{p}, f, \theta) - 10 \log d_{pq}}{10 \log d_{pq}} \right)^2 \quad (2)$$

where $\sigma^o_{pq}(\mathbf{X}; \mathbf{p}, f, \theta)$ and d_{pq} are, respectively, the calculated and measured backscattering coefficients of the area at the frequency f and observation angle θ for pq polarization, where $pq \in \{hh, vv, hv\}$. However, we only use the HH and VV channels in this paper due to the existing calibration uncertainties in the HV channel data. The vector $\mathbf{X}$ denotes the unknown parameters, namely $[a\ b\ c]^T$. Every other parameter necessary to characterize a radar pixel is assumed known and is represented in the vector $\mathbf{p}$. Section VI briefly describes these parameters.

The method of simulated annealing uses an analogy between the unknown parameters in the optimization problem and particles in the annealing process of solids. These particles are distributed randomly in the liquid phase at a high temperature. If cooling happens slowly enough, at each temperature T, the solid reaches thermal equilibrium, which is characterized by the Boltzmann distribution [36]. As the temperature decreases, the distribution concentrates on lower energy, and finally, when the temperature approaches zero, the only state that has a nonzero probability is the minimum energy state. In an optimization problem, the cost function and configurations of the model parameters are analogous to energy and different states of a solid, respectively. In an optimization algorithm based on simulated annealing, a small randomly generated perturbation is applied to the current model parameters $\mathbf{X}$. The new parameters are then used to calculate a new estimate of the backscattering coefficients, hence a new value for the cost function. If the cost function decreases, i.e., $\Delta L \leq 0$, the new state is accepted; otherwise, it is accepted with probability $e^{-\Delta L/T}$, where T is an inversion parameter referred to as temperature. This rule, referred to as the Metropolis criterion, is used at a sequence of decreasing temperatures. The simulated

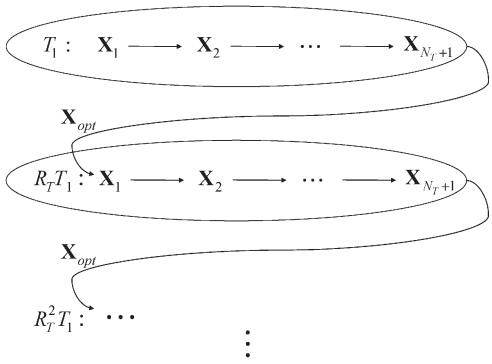

Fig. 6. Outline of the simulated annealing algorithm used in this paper. Step length is adjusted N_T times at each temperature before the temperature is reduced. The current state at each step length adjustment is denoted by $\mathbf{X}_2, \mathbf{X}_3, \ldots, \mathbf{X}_{N_T+1}$.

annealing algorithm implemented in this paper is based on the work by Corana *et al.* [35]. We start from an initial guess, an initial temperature, and an initial step length vector. A random move is generated sequentially along each coordinate direction. The trial point is either accepted or rejected according to the Metropolis criterion. This set of sequential perturbations is repeated N_s times. The step length is then adjusted according to the step length adjustment rule of the Corana *et al.* algorithm, and the iteration continues until the number of step length adjustments reaches N_T. The temperature is reduced at this point by $T_{\text{new}} = R_T T_{\text{old}}$, and the iteration continues at the new temperature starting from the current optimal point. This procedure is illustrated in Fig. 6, where the current state at each step length adjustment is denoted by $\mathbf{X}_2, \mathbf{X}_3, \ldots, \mathbf{X}_{N_T+1}$. Note that the first step length adjustment in each chain happens at $\mathbf{X}_2$ and the last one happens at $\mathbf{X}_{N_T+1}$, which is also the last accepted point of the corresponding chain. The inversion process stops when the cost function value becomes smaller than a value denoted by δ, i.e., $L \leq \delta$, when the number of forward function evaluations reaches a certain number, or when the algorithm converges to local minima for a certain number of times. (See [35] and [10] for more details on the inversion algorithm.)

Simulated annealing is a powerful global optimization technique that is capable of finding the global minimum hidden among many local minima. This method, like other global methods and unlike local optimization techniques, is insensitive to the initial guess, making it suitable for soil moisture retrieval. The potential of other global optimization methods such as the genetic algorithm and particle swarm can be studied and explored for the purpose of subsurface sensing. However, we have chosen to use simulated annealing in this paper because this method has proved powerful in an inversion problem associated with layered structures [10]. The study of other global techniques in the context of subsurface sensing can be the subject of another article.

To calculate the forward solution, we need the radar look angle, frequency, vegetation parameters, and soil texture information, all available as discussed in Section VI. We model the soil as a layered dielectric structure where the depth (or location) of the boundary of each modeled layer is calculated from the index number of that layer and the thickness of the overlying layers. The soil moisture of each layer is calculated from $m_v = az^2 + bz + c$, given the depth z and the current state of the polynomial coefficients a, b, and c. The texture of each layer is chosen depending on the location of its boundary within the actual soil layers. Soil texture properties (i.e., bulk density, and sand, silt, and clay densities) of the actual soil layers are based on the Soil Survey Geographic (SSURGO) database from which the actual number of soil layers and their thicknesses are available [37]. Finally, given the soil moisture and texture of each layer, the soil mixture model by Peplinski *et al.* is used to calculate the dielectric constant of that layer [38], [39].

The number of modeled soil layers and their thicknesses along with the simulated annealing parameters are chosen empirically based on the required accuracy and reasonableness of computational cost, and after extensive simulations using both synthetic and real radar data. The synthetic data inversion, described in Section VII-A, is mainly used to validate the mechanics of the inversion algorithm and to choose the appropriate simulated annealing parameters (such as the chain length, initial temperature, and stopping criterion), considering the limitations imposed by the available computational resources. These parameters are in turn used in a series of real data inversion (at the pixel where *in situ* soil moisture data are available) to choose the appropriate constraints on the unknown coefficients, number of layers, and their thicknesses, considering the retrieval depth preference (not requirement) for the Level 4 products. In this paper, we have used 11 layers with a thickness of 5 cm for each (i.e., retrieval depth of 50 cm) in the synthetic data inversion (see Section VII-A) and 20 layers with a thickness of 5 cm for each (i.e., retrieval depth of 95 cm) in the real data inversion (see Section VII-B).

We should mention that the unknown coefficients a, b, and c have different impacts on the radar response. For example, the coefficient c is the surface moisture $(m_v(0) = c)$; therefore, it will have more impact on the radar response when the soil has a wetter surface and drier depths, after a rain for example. On the other hand, the coefficient a determines the shape of the profile for deeper depths (as it multiplies z^2); therefore, it will have more impact on the radar response when we have drier surface and wetter depths. However, these different sensitivities do not make the optimization problem well posed because there are two data points (i.e., HH and VV channels) versus three unknowns, causing the problem to possibly have more than one global minimum, even if no noise contaminates the data. By imposing constraints on the coefficients based on *in situ* soil moisture data, we can mitigate the ill-conditioning of the problem and solve it successfully. For the real radar data inversions in this paper, and guided by available *in situ* soil moisture data, the coefficients have been constrained as $-3 \leq a \leq 3$, $-1 \leq b \leq 1$, and $0 \leq c \leq 0.2$. For synthetic data inversion and to study the behavior of the inversion algorithm, we have relaxed the constraints on b and c as $-3 \leq b \leq 3$, and $0 \leq c \leq 0.5$.

VI. Ancillary Data Layers and Site Description

Polarimetric P-band radar backscattering coefficients for each AirMOSS site are delivered by JPL at resolutions of

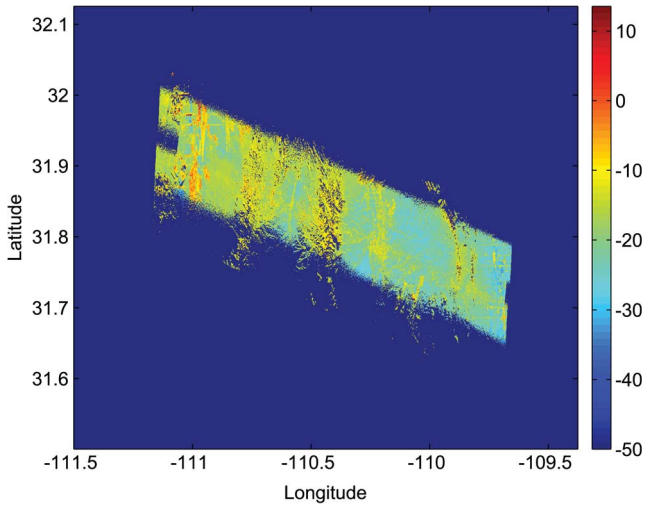

Fig. 7. Mosaicked radar image of the AirMOSS site in Arizona from October 23, 2012 for HH polarization. The values are in decibels. The blue area, i.e., −50 dB, is the image background.

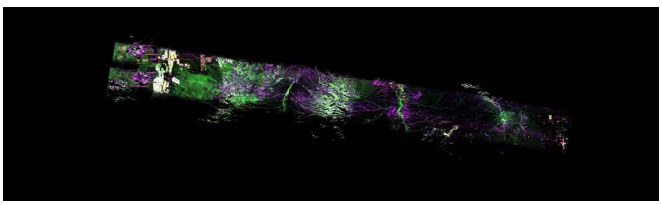

Fig. 8. RGB image of the radar backscatter over the AirMOSS site in Arizona from October 23, 2012. (Red: HH, Green: HV, Blue: VV).

0.5 and 3 arcseconds. The data are acquired by flying over an effective swath of approximately 25 km by 100 km. The effective swath is composed of several subswaths flown as separate flight lines. Each flight line covers a range of local incidence angles from approximately 25° to 55°. Fig. 7 shows an example of the mosaicked radar image for HH polarization at 3-arcsecond resolution from October 23, 2012, 5:30 A.M. over the AirMOSS site in Arizona, whereas Fig. 8 shows an RGB image of the radar backscatter.

The information necessary to characterize the pixels and their vegetation and soil geometry stems from readily available ancillary data used by the inversion algorithm to calculate the output of the forward model. The incidence angle and the slope of each pixel are included in the radar data at the same resolution. To generate the slope map, the digital elevation model (DEM) from the Shuttle Radar Topography Mission (SRTM) is used during the radar data processing [40]. For land cover type within the continental U.S., we use the most recent land cover map from the National Land Cover Database (NLCD) from the year 2006 [41]. For sites outside of the U.S., GlobCover data from the ESA GlobCover project are used [42]. The vegetation parameterization is based on land cover type only. For each land cover type, a standardized vegetation parameterization is determined based on data collected in the field. These data include vegetation geometric parameters such as height, Diameter at Breast Height (DBH), branch lengths, branch densities, branch diameters, leaf properties, and stem and branch dielectric constants. The soil roughness and temperature are determined based on field measurements, whereas other soil information is available from the SSURGO database

TABLE I
VEGETATION PARAMETERS OF A TYPICAL GRASSLAND PIXEL IN WALNUT GULCH

Parameter	*Value*	*Parameter*	*Value*
Canopy Height	0.65 m	SB Orientation	N/A
LB Dielectric	$12 - j3$	Leaf Dielectric	N/A
LB Length	7.00 cm	Leaf Thickness	N/A
LB Radius	0.0175 cm	Leaf Radius	N/A
LB Density	1720/m^3	Leaf Density	N/A
LB Orientation	35°	Stalk Dielectric	$12 - j3$
SB Dielectric	N/A	Stalk Length	5.00 cm
SB Length	N/A	Stalk Radius	0.0350 cm
SB Radius	N/A	Stalk Density	430/m^2
SB Density	N/A		

for the U.S. and from the Harmonized World Soil Database produced by the International Institute for Applied Systems Analysis (IIASA) for sites outside the U.S. [43]. The parameterization is validated by comparing the output of the forward model against radar data over several pixels within the same scene.

All ancillary data layers are postprocessed to a consistent 1 arcseconds (or ≃30 m) and then 3 arcseconds (or ≃90 m) resolution. The handling and processing of ancillary data is an involved process with many details that are beyond the scope of this paper. The data handling and processing strategy that enables large-scale RZSM estimation will be reported in a separate paper.

The study site we refer to as Walnut Gulch in this paper is located within the USDA-ARS Walnut Gulch Experimental Watershed near Tombstone, AZ. The dominant vegetation types within the study areas are grassland and shrubland. For the September 2012 flights, Kendall was selected as the ground sampling site for grassland, and Lucky Hills was selected as the ground sampling site for shrubland. Both Kendall and Lucky Hills are flux tower sites and have been monitored continuously for more than a decade. During overflight days, soil moisture and vegetation sampling was performed at both sites. For the October 2012 flights, the Empire Ranch study site was added to conduct more dedicated soil moisture sampling in shrubland. The September flight was conducted during the ending of the watershed wet season, and the October flight was during the beginning of its dry season, hence covering a range of soil moisture conditions. The topography of the sites is generally hilly with small slopes (smaller than 5°). There are often obvious trenches due to water flow during the wet season. The soil is hard and rocky, which limited the depth of moisture sampling and the number of samples that were collected.

The soil and vegetation parameters are typical parameters of the pixels in Walnut Gulch and have been measured directly in the field in support of the AirMOSS field campaigns. For locations where field data are not available, data from similar sites are used. Tables I–III summarize the vegetation parameters of the grassland, shrubland, and evergreen pixels, respectively. The soil texture parameters for all pixels and all depths are assigned as $S = 0.643$, $C = 0.106$, and $\rho_b = 1.55$ g/cm^3, where S, C, and ρ_b are, respectively, sand fraction, clay fraction, and bulk density of the soil. The look angle ranges from $\simeq 30°$ to $\simeq 52°$. These values are based on locations of such pixels within the AirMOSS radar swaths. The frequency is 430.3 MHz.

TABLE II
VEGETATION PARAMETERS OF A TYPICAL SHRUBLAND PIXEL IN WALNUT GULCH

Parameter	*Value*	*Parameter*	*Value*
Canopy Height	0.983 m	SB Orientation	30°
LB Dielectric	$15 - j3$	Leaf Dielectric	$15 - j3$
LB Length	0.492 m	Leaf Thickness	0.05 cm
LB Radius	0.4 cm	Leaf Radius	1.0 cm
LB Density	7.34/m^3	Leaf Density	1468/m^3
LB Orientation	60°	Trunk Dielectric	$15 - j3$
SB Dielectric	$15 - j3$	Trunk Length	5.0 cm
SB Length	0.246 m	Trunk Radius	0.4 cm
SB Radius	0.1 cm	Trunk Density	0.432/m^2
SB Density	29.36/m^3		

TABLE III
VEGETATION PARAMETERS OF A TYPICAL EVERGREEN PIXEL IN WALNUT GULCH

Parameter	*Value*	*Parameter*	*Value*
Canopy Height	11.4 m	SB Orientation	70°
LB Dielectric	$32 - j4$	Needle Dielectric	$32 - j4$
LB Length	1.2 m	Needle Length	3 cm
LB Radius	0.66 cm	Needle Radius	0.15 cm
LB Density	0.54/m^3	Needle Density	1728/m^3
LB Orientation	80°	Trunk Dielectric	$36 - j2$
SB Dielectric	$32 - j4$	Trunk Length	2.0 m
SB Length	0.8 m	Trunk Radius	6.8 cm
SB Radius	0.46 cm	Trunk Density	0.25/m^2
SB Density	0.54/m^3		

VII. INVERSION RESULTS AND DISCUSSION

We apply the inversion algorithm described in Section V to synthetic radar data to show the applicability of our method and to adjust the inversion algorithm parameters (such as the chain length, initial temperature, and stopping criterion). The algorithm is then applied to some real radar data (at the flux tower pixels where *in situ* soil moisture data are available) to choose the appropriate number of layers, their thicknesses, and constraints on the unknown coefficients. Finally, the inversion algorithm is applied to AirMOSS radar data acquired over the AirMOSS site in Arizona, including the Walnut Gulch Experimental Watershed. We would like to add that, given the parameters in Table III, the total one-way attenuation in the branch and trunk layers of an evergreen pixel in the site would be less than 1 dB for HH polarization, for example. This value is well above the system's equivalent sigma nought of $\simeq -40$ dB. Therefore, retrieval accuracy is not expected to be heavily affected by attenuation in the branch and trunk layers.

A. Inversion of Soil-Moisture Profile Using Synthetic Data

To validate the mechanics and implementation of the inversion method and to choose an appropriate set of inversion parameters, we first apply the method to synthetic data and then to nominal (but arbitrary) soil moisture profiles. The synthetic data used here are simulated with the model of [34], which is briefly explained in Section V. The radar data are assumed to have the following model:

$$\sigma_{pq}^{n} = \sigma_{pq} + r \tag{3}$$

where σ_{pq}^{n} represents the measured radar signal (in decibels), and σ_{pq} is the error-free radar signal (in decibels) simulated with the forward model. The quantity r is a random number uniformly distributed between -1 and 1. Considering the calibration errors explained in Section II, r would be an overestimation of the calibration error. This overestimation is necessary to account for errors in the ancillary data and the scattering model. We will see in Section VII-B that the RMSE figures in this analysis are overestimated of the errors present in the retrieval results when real radar data are used.

We demonstrate the inversion method using two different pixels, namely bare soil and shrubs. The parameters characterizing pixels are from Walnut Gulch data described in Section VI. However, the moisture profiles used in the simulations are the same profiles shown in Fig. 2(b). We have used 11 layers with a thickness of 5 cm for each to discretize the moisture profile.

The inversion algorithm is applied to 300 realizations of the perturbed data modeled with (3), and the PDF of the RMSE between the retrieved and actual profiles is calculated. Fig. 9 shows these results. The average RMSEs for all profiles are shown, which we reiterate are overestimation of the errors observed with real radar data. We should mention that the PDF is plotted by smoothing the histogram of the output, resulting in negative RMSE for some of the realizations.

B. Inversion of Soil-Moisture Profile From AirMOSS Data

We use the AirMOSS data from three different dates, namely September 20, October 23, and October 29, 2012, acquired over the Arizona site. The flown area comprises hundreds of thousands of 3-arcsecond pixels. Specifically, the radar images from September 20, October 23, and October 29, 2012 contain, respectively, 515 867, 364 772, and 421 700 pixels. However, due to several masks that we apply to the radar data, only 411 337, 240 859, and 307 946 are enabled for inversion, respectively. The 3-arcsecond pixels that are disabled (or masked out) are the pixels that: 1) are classified by the NLCD as water, ice/snow, developed space (open space, low/medium/high intensity), woody wetlands, or any of the wetland classes; or 2) have a slope of more than 10°. Currently, some additional pixels are masked out due to nonexisting SSURGO data. In the future, we will use soil products that are gap filled with the State Soil Geographic (STATSGO) data [44]. Moreover, pixels with bedrock, water features, river washes, rough broken land, rocky outcrop, or lava fields, which have no soil characteristics, are also masked out.

The simulated annealing algorithm is rather computationally expensive, because it often requires thousands of forward-model runs per pixel. However, since each pixel can be inverted independently, it is possible to retrieve the soil moisture profile coefficients for the entire image in a reasonable length of time by dividing the image into several segments and performing the processing on a high-performance computing cluster. Currently, we are utilizing two clusters, namely the High Performance Computing and Communications (HPCC) supercomputer cluster at the University of Southern California and the High-End Computing Capability (HECC) cluster at the NASA Ames Research Center. Each utilized HPCC node has two 2.3-GHz Dodecacore AMD Opteron processors with 48 GB of memory.

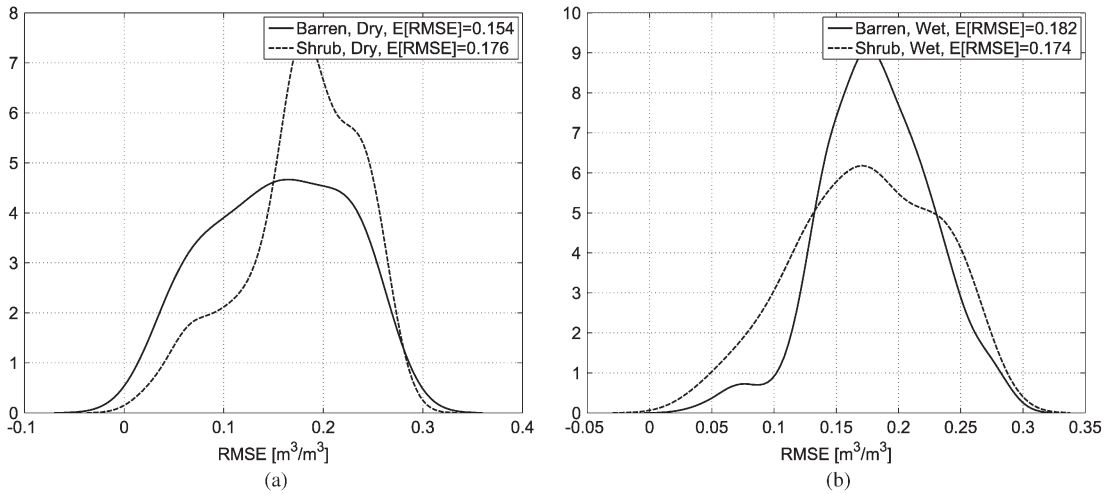

Fig. 9. Of the RMSE between the retrieved and actual profiles for two typical moisture profiles shown in Fig. 2(b) and two typical pixels (i.e., barren and shrubland) in the Walnut Gulch site using synthetic radar data. The average RMSEs are shown on the plots. (a) Dry profile. (b) Wet profile.

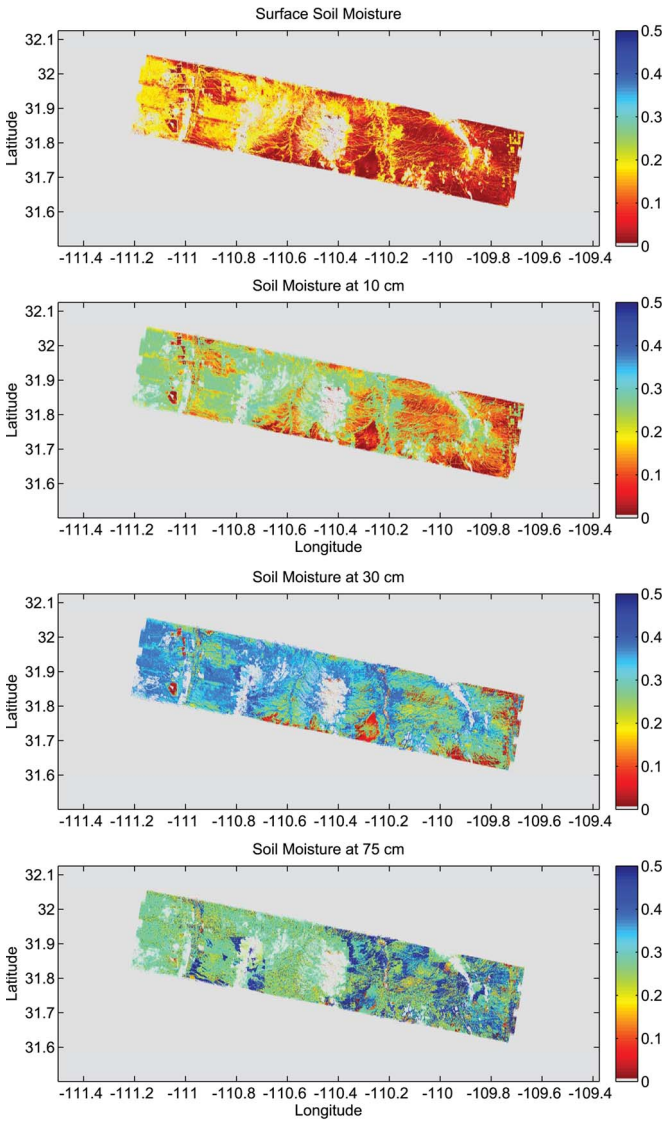

Fig. 10. Map of soil moisture of the AirMOSS site in Arizona at four sample depths of 0, 10, 30, and 75 cm estimated by the inversion algorithm for September 20, 2012. The gray area, i.e., 0 m^3/m^3, is the image background.

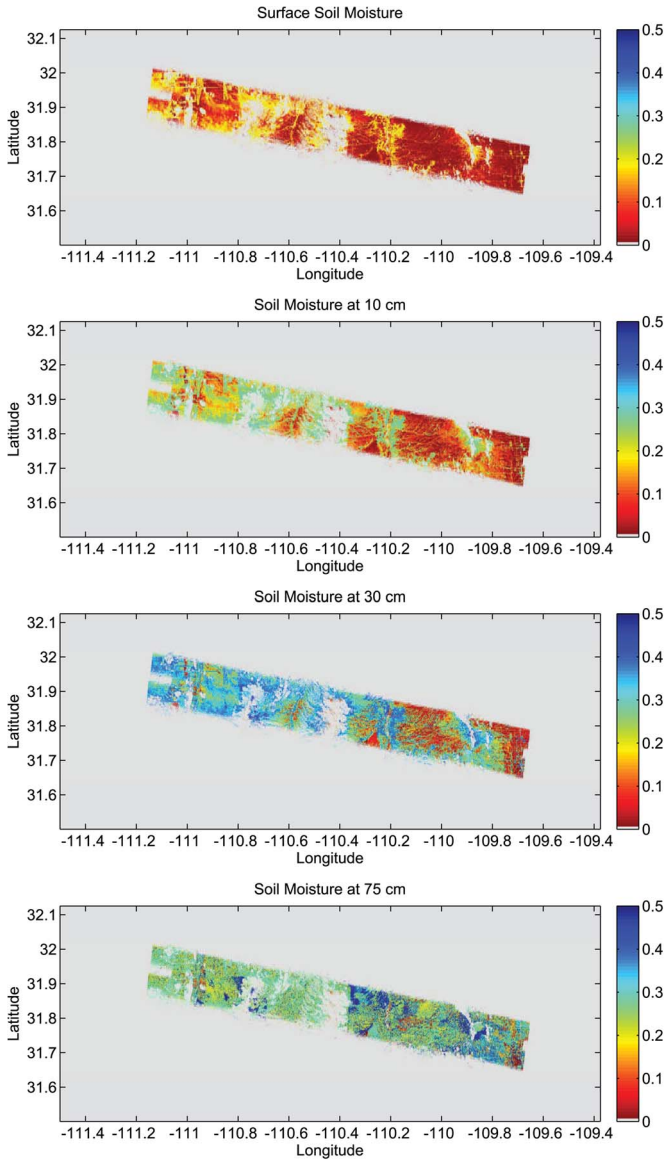

Fig. 11. Map of soil moisture of the AirMOSS site in Arizona at four sample depths of 0, 10, 30, and 75 cm estimated by the inversion algorithm for October 23, 2012. The gray area, i.e., 0 m^3/m^3, is the image background.

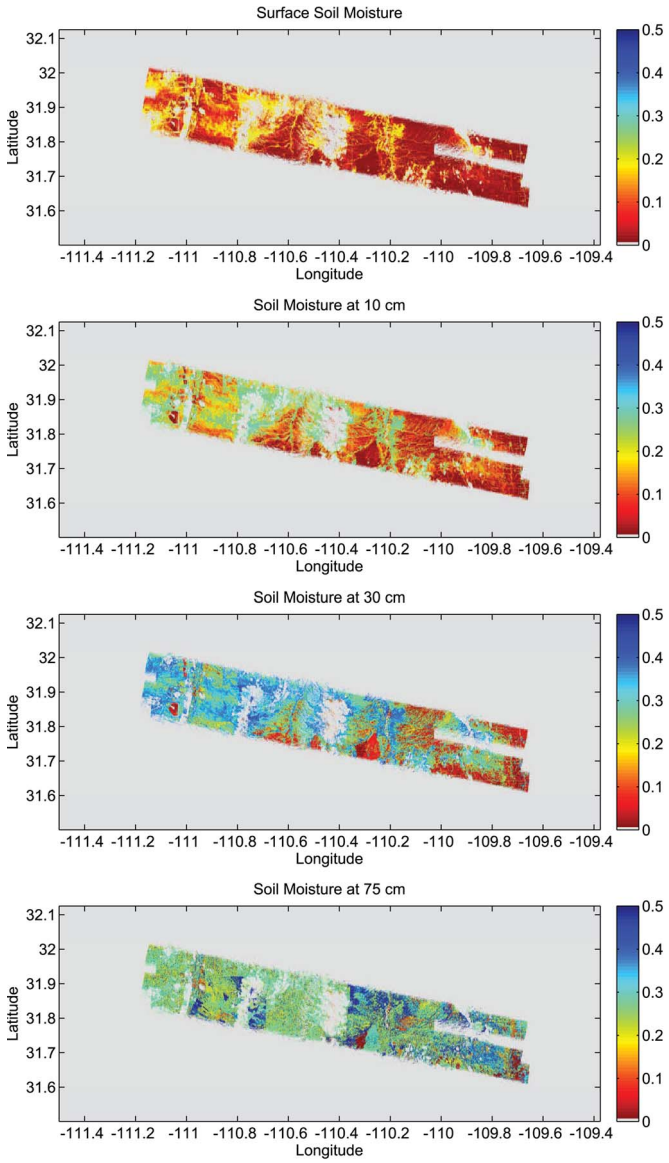

Fig. 12. Map of soil moisture of the AirMOSS site in Arizona at four sample depths of 0, 10, 30, and 75 cm estimated by the inversion algorithm for October 29, 2012. The gray area, i.e., 0 $\mathrm{m}^3/\mathrm{m}^3$, is the image background.

Each utilized HECC node has two 3-GHz Quadcore Intel Xeon processors with 8 GB of memory.

Figs. 10–12 show the soil moisture maps of the AirMOSS site in Arizona at four sample depths of 0, 10, 30, and 75 cm for September 20, October 23, and October 29, 2012. For this set of inversions, we have used 20 layers, with a thickness of 5 cm for each, to discretize the unknown profile, making the results valid up to 95 cm.

To validate the inversion results, we use the data collected by USDA from probes originally installed in support of the MOSS project in 2002–2004. These probes are near the Lucky Hills Shrubland and Kendall Grassland flux towers within the watershed. Multiple soil moisture profiles are installed at each location, and the probes along each profile are at various depths. For example, one profile has probes at the depths of 5, 15, and 38 cm, whereas another profile probes the soil moisture at the depths of 0, 5, 15, 30, 75, and 100 cm. The validation plots below show these various depths for the profiles. The probes collect data every 30 min throughout the day and year. We have compared the retrieved soil moisture profiles against the available soil moisture data for the three dates mentioned earlier at both Lucky Hills Shrubland and Kendall Grassland. Figs. 13–15 show these comparisons, in which RMSE has been calculated over the depths smaller than 95 cm. The data collected by probes are sometimes corrupted or invalid (i.e., nonphysical) due to hardware or recording problems. Therefore, the validation results are only shown for valid *in situ* data. For September 20, 2012, the average RMSEs over all probes for Lucky Hills Shrubland and Kendall Grassland are 0.037 and 0.095 $\mathrm{m}^3/\mathrm{m}^3$, respectively, and 0.060 $\mathrm{m}^3/\mathrm{m}^3$ over both areas. For October 23, the retrieved profile is generally underestimating the soil moisture, and the average RMSEs over all probes for Lucky Hills Shrubland and Kendall Grassland are 0.070 and 0.046 $\mathrm{m}^3/\mathrm{m}^3$, respectively, and 0.064 $\mathrm{m}^3/\mathrm{m}^3$ over both areas. For October 29, the retrieved profile is generally overestimating the soil moisture, and the average RMSEs over all probes for Lucky Hills Shrubland and Kendall Grassland are 0.105 and 0.064 $\mathrm{m}^3/\mathrm{m}^3$, respectively, and 0.099 $\mathrm{m}^3/\mathrm{m}^3$ over both areas. The average RMSE over all profiles, all dates, and both sites is 0.075 $\mathrm{m}^3/\mathrm{m}^3$. The breakdown of these results is summarized in Table IV.

The validation plots suggest that we should investigate the level of confidence in the retrieval results for different depth thresholds. We examine two thresholds, namely 50 and 30 cm. For each date, we calculate the RMSE over all profiles in both sites, i.e., Lucky Hills Shrubland and Kendall Grassland. Table V shows the summary. The accuracy in the retrieval increases if RMSE is calculated based on points closer to the surface, indicating more confidence in the retrieval for such points. It should be mentioned that, in the calculation of RMSE, we have not removed any biases in the retrieved soil moisture values, and the RMSE is calculated as

$$\mathrm{RMSE} = \sqrt{\frac{\sum_{i=0}^{N}(m_v - \widehat{m_v})^2}{N}} \tag{4}$$

where m_v is the measured soil moisture, $\widehat{m_v}$ is the estimated soil moisture, and N is the total number of probes used in the calculation of the RMSE. The possible radar calibration errors, inaccuracies in vegetation parameterization and modeling, surface roughness assumptions, and inaccuracies in the scattering and inversion models have contributed to the retrieval errors. Investigation and reduction of these errors is beyond the scope of this paper. With longer term data sets over the course of the AirMOSS mission, we would be able to reduce the aforementioned sources of uncertainty and to determine any site-dependent or uniform bias in the retrieved soil moisture values.

VIII. Summary and Conclusion

We presented a comprehensive description of the retrieval method used for mapping the RZSM in several AirMOSS sites. Brief overview of ancillary data and the study site was presented. Since the number of AirMOSS SAR observations is limited, to estimate deep soil moisture, rather than modeling soil moisture profile with several layers with unknown volumetric moisture contents, we modeled the unknown soil moisture

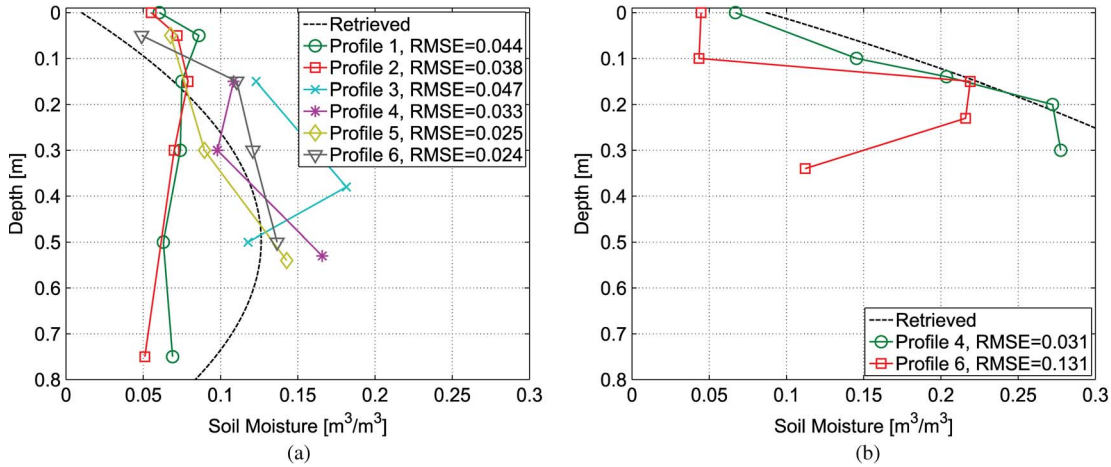

Fig. 13. Comparison between the retrieved and measured profiles on September 20, 2012 at 6:30 A.M. in (a) Walnut Gulch Lucky Hills Shrubland and (b) Walnut Gulch Kendall Grassland. The RMSE is calculated based on depths smaller than 95 cm. For Kendall Grassland, only two profiles reported valid data on this date.

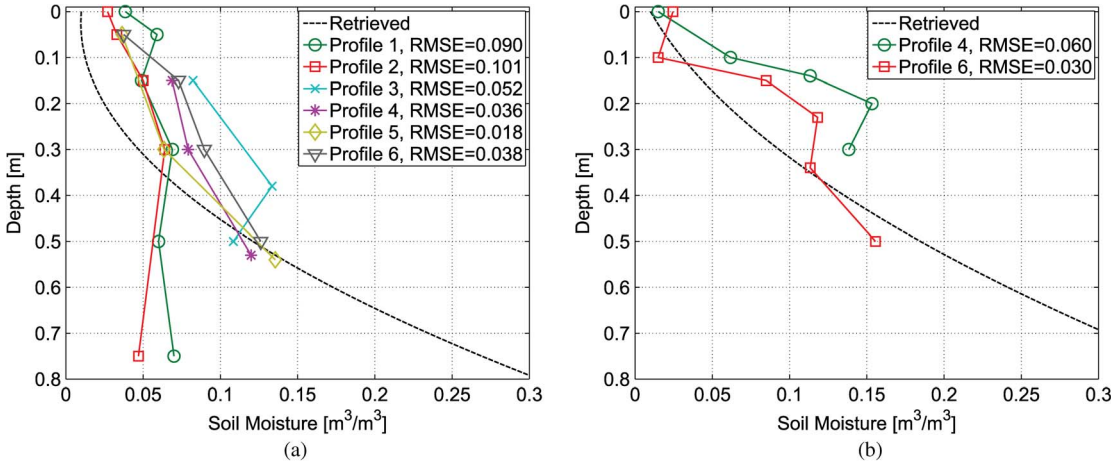

Fig. 14. Comparison between the retrieved and measured profiles on October 23, 2012 at 5:30 A.M. in (a) Walnut Gulch Lucky Hills Shrubland and (b) Walnut Gulch Kendall Grassland. The RMSE is calculated based on depths smaller than 95 cm. For Kendall Grassland, only two profiles reported valid data on this date.

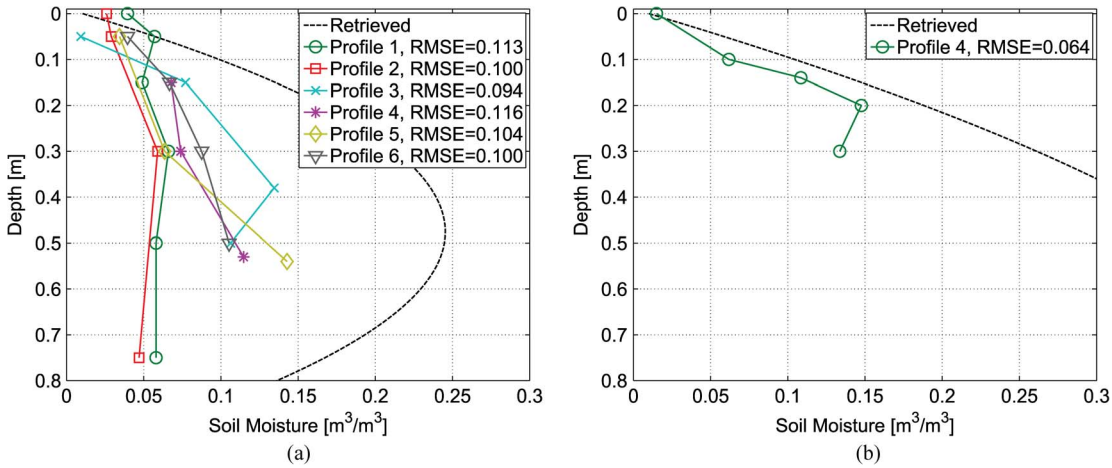

Fig. 15. Comparison between the retrieved and measured profiles on October 29, 2012 at 6:00 A.M. in (a) Walnut Gulch Lucky Hills Shrubland and (b) Walnut Gulch Kendall Grassland. The RMSE is calculated based on depths smaller than 95 cm. For Kendall Grassland, only one profile reported valid data on this date.

profile with a second-order polynomial with three coefficients. These coefficients were estimated with the simulated annealing method where the backscattering coefficients of the radar pixel, hence the cost function, were calculated using a single-species discrete radar scattering model. The ancillary data characterizing each pixel, i.e., vegetation and soil parameters, are acquired from several sources and are handled and prepared for the inversion algorithm in an involved process that will be detailed in a separate paper. Considering the required accuracy and reasonableness of the computational cost and guided by *in situ* field observations from several sites and prior field campaigns, the inversion algorithm parameters, including the number and thickness of the modeled soil layers' that discretize the unknown profile, were chosen empirically after extensive

TABLE IV
BREAKDOWN OF RMSE FOR WALNUT GULCH SITES

Date	*Lucky Hills Shrubland*	*Kendall Grasslands*	*Both Sites*
September 20	0.037	0.095	0.060
October 23	0.070	0.046	0.064
October 29	0.105	0.064	0.099
All Dates	0.076	0.072	0.075

TABLE V
RMSE FOR WALNUT GULCH (VARIOUS DEPTH THRESHOLDS)

Date	*RMSE (all points)*	*RMSE ($\leq$ 50 cm)*	*RMSE ($\leq$ 30 cm)*
September 20	0.060	0.063	0.045
October 23	0.064	0.041	0.042
October 29	0.099	0.096	0.084
All Dates	0.075	0.068	0.058

simulations using synthetic and real radar data. We applied the estimation algorithm to the radar data acquired over the AirMOSS site in Arizona from September and October of 2012. The retrieval accuracy was quantified based on the RMSE between estimated and measured profiles at locations within the Walnut Gulch Experimental Watershed where soil moisture probes are installed and soil moisture is monitored throughout the year. The validation results showed accuracy ranging from 0.041 to 0.099 m^3/m^3 while confirming the intuitive notion that the accuracy decreases as depth increases. The profiles used for validation are from a fairy dry season in Walnut Gulch and so are the accuracy conclusions. We showed in Section III that the second-order polynomial representation is still a good assumption for wet profiles. Nevertheless, we expect that the second-order polynomial would be more accurate in dry conditions. The validation of the algorithm will be extended to wet conditions in the future pending radar data from wet seasons. The existing uncertainty in the retrieval results are associated with radar calibration errors, vegetation parameterization and modeling errors, surface roughness assumptions, and inaccuracies in the scattering and inversion models. We should also mention that no biases have been removed in the calculation of RMSE. The biases present in the retrieved values of soil moisture can be due to the *in situ* probes, radar calibration, vegetation parameterization, forward-model inaccuracies, and the bias in the inversion algorithm. To determine whether a bias exists and whether this bias is site dependent, we would need to recalculate these errors with longer-term data sets over the course of the AirMOSS mission.

ACKNOWLEDGMENT

The authors would like to thank Dr. E. Chapin and J. Shimada from JPL for the information on the AirMOSS radar instrument, and the reviewers for their thorough and helpful comments.

REFERENCES

[1] R. D. Koster *et al.*, "Regions of strong coupling between soil moisture and precipitation," *Science*, vol. 305, no. 5687, pp. 1138–1140, Aug. 2004.
[2] D. Entekhabi *et al.*, "The soil moisture active and passive (SMAP) mission," *Proc. IEEE*, vol. 98, no. 5, pp. 704–716, May 2010.
[3] Airborne Microwave Observatory of Subcanopy and Subsurface (AirMOSS), Jet Propulsion Laboratory. [Online]. Available: https://airmoss.jpl.nasa.gov/
[4] Y. H. Kerr *et al.*, "The SMOS mission: New tool for monitoring key elements of the global water cycle," *Proc. IEEE*, vol. 98, no. 5, pp. 666–687, May 2010.
[5] F. T. Ulaby, "Radar measurement of soil moisture content," *IEEE Trans. Antennas Propag.*, vol. AP-22, no. 2, pp. 257–265, Mar. 1974.
[6] Y. Oh, K. Sarabandi, and F. T. Ulaby, "An empirical model and an inversion technique for radar scattering from bare soil surfaces," *IEEE Trans. Geosci. Remote Sens.*, vol. 30, no. 2, pp. 370–381, Mar. 1992.
[7] P. C. Dubois, J. van Zyl, and T. Engman, "Measuring soil moisture with imaging radars," *IEEE Trans. Geosci. Remote Sens.*, vol. 33, no. 4, pp. 915–926, Jul. 1995.
[8] M. Moghaddam, S. Saatchi, and R. H. Cuenca, "Estimating subcanopy soil moisture with radar," *J. Geophys. Res.*, vol. 105, no. D11, pp. 14 899–14 911, Jun. 2000.
[9] J. Shi, J. Wang, A. Y. Hsu, P. E. O'Neill, and E. T. Engman, "Estimation of bare surface soil moisture and surface roughness parameter using L-band SAR image data," *IEEE Trans. Geosci. Remote Sens.*, vol. 35, no. 5, pp. 1254–1266, Sep. 1997.
[10] A. Tabatabaeenejad and M. Moghaddam, "Inversion of subsurface properties of layered dielectric structures with random slightly-rough interfaces using the method of simulated annealing," *IEEE Trans. Geosci. Remote Sens.*, vol. 47, no. 7, pp. 2035–2046, Jul. 2009.
[11] S.-B. Kim *et al.*, "Models of L-band radar backscattering coefficients over the global terrain for soil moisture retrieval," *IEEE Trans. Geosci. Remote Sens.*, vol. 52, no. 2, pp. 1381–1396, Feb. 2014.
[12] Z. S. Haddad and P. Dubois, "Bayesian estimation of soil parameters from remote sensing data," in *Proc. IEEE IGARSS*, Pasadena, CA, USA, Aug. 1994, pp. 1421–1423.
[13] Y. Kim and J. J. van Zyl, "A time-series approach to estimate soil moisture using polarimetric radar data," *IEEE Trans. Geosci. Remote Sens.*, vol. 47, no. 8, pp. 2519–2527, Aug. 2009.
[14] S.-B. Kim *et al.*, "Soil moisture retrieval using time-series radar observations over bare surfaces," *IEEE Trans. Geosci. Remote Sens.*, vol. 50, no. 5, pp. 1853–1863, May 2012.
[15] M. Piles, D. Entekhabi, and A. Camps, "A chanage detection algorithm for retrieving high-resolution soil moisture from SMAP radar and radiometer observations," *IEEE Trans. Geosci. Remote Sens.*, vol. 47, no. 12, pp. 4125–4131, Dec. 2009.
[16] J. P. Walker, P. A. Troch, M. Mancini, G. R. Willgoose, and J. D. Kalma, "Profile soil moisture estimation using the modified IEM," in *Proc. IEEE IGARSS*, Singapore, Aug. 1997, pp. 1263–1265.
[17] D. Entekhabi, H. Nakamura, and E. G. Njoku, "Solving the inverse problem for soil moisture and temperature profiles by sequential assimilation of multifrequency remotely sensed observations," *IEEE Trans. Geosci. Remote Sens.*, vol. 32, no. 2, pp. 438–448, Mar. 1994.
[18] J. F. Galantowicz, D. Entekhabi, and E. G. Njoku, "Tests of sequential data assimilation for retrieving profile soil moisture and temperature from observed L-band radiobrightness," *IEEE Trans. Geosci. Remote Sens.*, vol. 37, no. 4, pp. 1860–1870, Jul. 1999.
[19] R. Hoeben and P. A. Troch, "Assimilation of active microwave measurements for soil moisture profile retrieval under laboratory conditions," in *Proc. IEEE IGARSS*, Honolulu, HI, USA, Jul. 2000, pp. 1271–1273.
[20] G. Ijjas, K. S. Rao, and Y. S. Rao, "Efficiency of 1.4 and 2.7 GHz radiometers data for the retrieval of soil moisture profile," in *Proc. IEEE IGARSS*, Helsinki, Finland, Jun. 1991, pp. 765–768.
[21] S. Paloscia, G. Macelloni, E. Santi, and M. Tedesco, "The capability of microwave radiometers in retrieving soil moisture profiles: An application of Artificial Neural Networks," in *Proc. IEEE IGARSS*, Toronto, ON, Canada, Jun. 2002, pp. 1390–1392.
[22] A. Tabatabaeenejad and M. Moghaddam, "Bistatic scattering from dielectric structures with two rough boundaries using the Small Perturbation Method," *IEEE Trans. Geosci. Remote Sens.*, vol. 44, no. 8, pp. 2102–2124, Aug. 2006.
[23] U. K. Khankhoje, J. van Zyl, Y. Kim, and T. Cwik, "Using polarimetric SAR data to infer soil moisture from surfaces with varying subsurface moisture profiles," in *Proc. IEEE IGARSS*, Munich, Germany, Jul. 2012, pp. 1453–1456.
[24] A. Tabatabaeenejad, X. Duan, and M. Moghaddam, "Coherent scattering of electromagnetic waves from two-layer rough surfaces within the Kirchhoff regime," *IEEE Trans. Geosci. Remote Sens.*, vol. 51, no. 7, pp. 3943–3953, Jul. 2013.
[25] E. A. Reutov and A. M. Shutko, "Prior-knowledge-based soil moisture determination by microwave radiometry," *Soviet J. Remote Sens.*, vol. 5, no. 1, pp. 100–125, 1986.
[26] G. D. Salvucci, "An approximate solution for steady vertical flux of moisture through an unsaturated homogeneous soil," *Water Resour. Res.*, vol. 29, no. 11, pp. 3749–3753, Nov. 1993.

[27] A. Tabatabaeenejad, M. Burgin, and M. Moghaddam, "Impact of subsurface layers on subcanopy soil moisture retrieval from radar," presented at the IEEE IGARSS, Munich, Germany, Jul. 2012.
[28] D. Entekhabi and M. Moghaddam, "Mapping recharge from space: Roadmap to meeting the grand challenge," *Hydrogeol. J.*, vol. 15, no. 1, pp. 105–116, Feb. 2007.
[29] E. Chapin *et al.*, "AirMOSS: An airborne P-band SAR to measure root-zone soil moisture," in *Proc. IEEE Radar Conf.*, Atlanta, GA, USA, May 2012, pp. 693–698.
[30] The Boreal Ecosystem-Atmosphere Study (BOREAS), The Oak Ridge National Laboratory Distributed Active Archive Center. [Online]. Available: http://daac.ornl.gov/BOREAS/boreas.shtml
[31] M. Moghaddam *et al.*, "Microwave Observatory of Subcanopy and Subsurface (MOSS): A mission concept for global deep soil moisture observations," *IEEE Trans. Geosci. Remote Sens.*, vol. 45, no. 8, pp. 2630–2643, Aug. 2007.
[32] S. L. Durden, J. J. Van Zyl, and H. A. Zebker, "Modeling and observation of the radar polarization signature of forested areas," *IEEE Trans. Geosci. Remote Sens.*, vol. 27, no. 3, pp. 290–301, May 1989.
[33] M. Burgin, D. Clewley, R. M. Lucas, and M. Moghaddam, "A generalized radar backscattering model based on wave theory for multilayer multispecies vegetation," *IEEE Trans. Geosci. Remote Sens.*, vol. 49, no. 12, pp. 4832–4845, Dec. 2011.
[34] M. Burgin, A. Tabatabaeenejad, and M. Moghaddam, "A generalized radar scattering model for multispecies forests with multilayer subsurface soil," in *Proc. IEEE IGARSS*, Munich, Germany, Jul. 2012, pp. 5817–5819.
[35] A. Corana, M. Marchesi, C. Martini, and S. Ridella, "Minimizing multimodal functions of continuous variables with the 'Simulated Annealing' algorithm," *ACM Trans. Math. Softw.*, vol. 13, no. 3, pp. 262–280, Sep. 1987.
[36] S. Kirkpatrick, C. D. Gelatt, and M. P. Vecchi, "Optimization by simulated annealing," *Science*, vol. 220, no. 4598, pp. 671–680, May 1983.
[37] Soil Survey Geographic (SSURGO), Natural Resources and Conservation Service (NRCS). [Online]. Available: http://soils.usda.gov/survey/geography/ssurgo/
[38] N. R. Peplinski, F. T. Ulaby, and M. C. Dobson, "Dielectric properties of soils in the 0.3–1.3-GHz range," *IEEE Trans. Geosci. Remote Sens.*, vol. 33, no. 3, pp. 803–807, May 1995.
[39] N. R. Peplinski, F. T. Ulaby, and M. C. Dobson, "Corrections to "Dielectric properties of soils in the 0.3–1.3-GHz range"," *IEEE Trans. Geosci. Remote Sens.*, vol. 33, no. 6, p. 1340, Nov. 1995.
[40] Jet Propulsion Laboratory, The Shuttle Radar Topography Mission (SRTM). [Online]. Available: http://www2.jpl.nasa.gov/srtm/
[41] Multi-Resolution Land Characteristics Consortium (MRLC), National Land Cover Database (NLCD) 2006. [Online]. Available: http://www.mrlc.gov/nlcd06_data.php/
[42] European Space Agency (ESA), European Space Agency GlobCover Portal. [Online]. Available: http://due.esrin.esa.int/globcover/
[43] International Institute for Applied Systems Analysis (IIASA), Harmonized World Soil Database. [Online]. Available: http://webarchive.iiasa.ac.at/Research/LUC/External-World-soil-database/HTML/
[44] Natural Resources and Conservation Service (NRCS), U.S. General Soil Map (STATSGO2). [Online]. Available: http://soildatamart.nrcs.usda.gov

Alireza Tabatabaeenejad (S'98–M'09–SM'14) received the B.S. degree from the Sharif University of Technology, Tehran, Iran, in 2001 and the M.S. and Ph.D. degrees from the University of Michigan, Ann Arbor, MI, USA, in 2003 and 2008, respectively, all in electrical engineering.

From 2009 to 2011, he was a Postdoctoral Research Fellow with the Radiation Laboratory, University of Michigan. He is currently a Research Assistant Professor with the Ming Hsieh Department of Electrical Engineering, University of Southern California (USC), Los Angeles, CA, USA. His research interests include radar remote sensing and electromagnetic scattering.

Dr. Tabatabaeenejad is currently serving as Secretary of the IEEE Geoscience and Remote Sensing Society Chapter in the Metropolitan Los Angeles Section.

Mariko Burgin (S'09–M'14) received the M.S. degree in electrical engineering and information technology from the Swiss Federal Institute of Technology (ETH), Zurich, Switzerland, in 2008 and the M.S. and Ph.D. degrees in electrical engineering from the University of Michigan, Ann Arbor, MI, USA, in 2011 and 2014, respectively.

She is currently a Postdoctoral Scholar with the Water and Carbon Cycles Group, NASA Jet Propulsion Laboratory, California Institute of Technology, Pasadena, CA, USA. Her research interests include theoretical and numerical studies of random media, development of forward and inverse scattering algorithms for soil moisture retrieval, and the study of electromagnetic wave propagation and scattering properties of vegetated surfaces.

Xueyang Duan (S'07–M'12) received the B.Eng. degree in communication engineering from Shandong University, Jinan, China, in 2004; the M.S. degree in microelectronics and communications technology from the University of Ulm, Ulm, Germany, in 2006; and the M.S. degree in applied mathematics and the Ph.D. degree from the University of Michigan, Ann Arbor, MI, USA, in 2010 and 2012, respectively.

From 2006 to 2007, she was with the Test and Measurement Division, Rohde & Schwarz, Munich, Germany, as a Development Engineer for vector network analyzers. She spent two years as a Postdoctoral Research Associate with the Department of Electrical Engineering, University of Southern California, Los Angeles, CA, USA. Since 2014, she has been with the NASA Jet Propulsion Laboratory, California Institute of Technology, Pasadena, CA. Her research interests include forward and inverse modeling of electromagnetic scattering from layered rough surfaces with or without buried objects, radar system design, and radar measurements of vegetation and ground variables.

Mahta Moghaddam (S'86–M'87–SM'02–F'09) received the B.S. degree (with the highest distinction) from the University of Kansas, Lawrence, KS, USA, in 1986 and the M.S. and Ph.D. degrees from the University of Illinois at Urbana-Champaign, Champaign, IL, USA, in 1989 and 1991, respectively, all in electrical and computer engineering.

From 1991 to 2003, she was with the Radar Science and Engineering Section, NASA Jet Propulsion Laboratory (JPL), California Institute of Technology, Pasadena, CA, USA. From 2003 to 2011, she was a Professor of electrical engineering and computer science with the University of Michigan, Ann Arbor, MI, USA. She was a Systems Engineer for the Cassini Radar, the JPL Science Group Lead for the LightSAR Project, and the Science Chair of the JPL Team X (Advanced Mission Studies Team). She has introduced new approaches for quantitative interpretation of multichannel radar imagery based on analytical inverse scattering techniques applied to complex and random media. She is currently a Professor of electrical engineering with the Ming Hsieh Department of Electrical Engineering, University of Southern California, Los Angeles, CA. Her current research interests include the development of new radar instrument and measurement technologies for subsurface and subcanopy characterization, development of forward and inverse scattering techniques of layered random media, and transforming concepts of radar remote sensing to near-field and medical imaging and therapy systems. She is a member of the NASA Soil Moisture Active and Passive (SMAP) mission Science Team, the Chair of the SMAP Algorithms Working Group, a member of the NASA Advisory Council Earth Science Subcommittee, and the Principal Investigator of the AirMOSS Earth Ventures 1 Mission.